Fe_2O_3-graphitic carbon nitride nanocomposites analyzed by XPS

Mattia Benedet,[1,2,a)] Davide Barreca,[2,a)] Gian Andrea Rizzi,[1,2] Chiara Maccato,[1,2] Jan-Lucas Wree,[3] Anjana Devi,[3] and Alberto Gasparotto,[1,2]

[1] *Department of Chemical Sciences, Padova University and INSTM, 35131 Padova, Italy*
[2] *CNR-ICMATE and INSTM, Department of Chemical Sciences, Padova University, 35131 Padova, Italy*
[3] *Inorganic Materials Chemistry, Ruhr University Bochum, Bochum, Germany*

(Received day Month year; accepted day Month year; published day Month year)

Nanocomposite systems based on iron(III) oxide (Fe_2O_3) and graphitic carbon nitride (gCN) possess a great potential as photo(electro)catalysts for environmental remediation and energy generation. In this field, a key issue is the fabrication of supported materials directly grown onto suitable substrates and possessing tailored features. In the present study, Fe_2O_3-gCN nanomaterials are prepared by an innovative two-step strategy, consisting in the initial plasma assisted-chemical vapor deposition (PA-CVD) of iron(III) oxide on conducting glass substrates and the subsequent functionalization with low amounts of gCN by a facile electrophoretic deposition (EPD) process. Attention is dedicated to the use of two different forms of carbon nitride, obtained from melamine or melamine + cyanuric acid, in order to finely tune the resulting material composition. In this work, X-ray photoelectron spectroscopy (XPS) was used to characterize the pristine Fe_2O_3 deposit, as well as two Fe_2O_3-gCN composite materials prepared starting from different gCN powders. A detailed analysis of the obtained spectroscopic data reveals the occurrence of a direct electronic interplay between the single constituents, dependent on material characteristics. The related results may act as useful guidelines for the design of photo(electro)catalysts endowed with specific properties, of importance for sustainable applications.

Keywords: Fe_2O_3; graphitic carbon nitride; PA-CVD; electrophoretic deposition; X-ray photoelectron spectroscopy

Acccession#:01865, 01866, and 01867

Technique: XPS

Host Material: Fe_2O_3; Fe_2O_3-gCN(M); Fe_2O_3-gCN(CM)

Instrument: PHI 5000 Versaprobe

Major Elements in Spectra: C, N, O, Fe

Minor Elements in Spectra: none

Published Spectra: 14

Spectra in Electronic Record: 14

Spectral Category: comparison

INTRODUCTION

Over the last decade, the increasing concern in environmental and human health safeguard has stimulated efforts dedicated to the fabrication of eco-friendly photoactive materials capable of triggering pollutant decomposition into harmless products and of promoting sustainable energy generation from natural resources. Among the possible candidates, hematite (α-Fe_2O_3) is one of the most promising materials due to its economic viability, abundance, stability, and band gap in the visible spectral range, enabling to efficiently harvest the largely available sunlight to trigger the target processes (Refs. 1-6). Yet, large-scale real-world applications of hematite as such are precluded by the detrimental recombination of photogenerated electrons and holes, limiting the overall efficiency (Refs. 1, 3, 4, 7-10). To circumvent these disadvantages, attractive options are provided by the controllable constructions of heterojunctions with suitable semiconductors, among which graphitic carbon nitride (gCN) features a variety of profitable properties - encompassing structural and chemical flexibility, tuneable defectivity and moderate band gap ($E_G \approx$ 2.4-2.8 eV) (Refs. 11-20). To suppress the recombination of charge carriers affecting even gCN, a valuable opportunity is offered by its integration with metal oxides to yield Fe_2O_3-gCN heterostructures (Ref. 9, 11, 15, 17, 19-26). Indeed, similar systems have been successfully utilized for the manufacturing of photo(electro)catalysts aimed at pollutant degradation (Ref. 9, 13, 14, 17, 21, 22, 27, 28), CO_2 reduction to solar fuels (Refs. 16, 29) and for the production of molecular hydrogen (H_2), a strategically appealing energy vector (Refs. 2, 7, 11, 12, 24, 30).

Future research advancements for the eventual implementation of the above materials in practical applications inevitably require their direct growth onto suitable substrates, at variance with the use of systems in powdered form (or fabricated through powders immobilization on substrates (Refs. 20, 27, 31). In this regard, a technologically appealing preparation route should offer not only various degrees of freedom to effectively modulate material structure, composition and morphology (Ref. 31), but also the possibility of obtaining an intimate interfacial contact between Fe_2O_3 and gCN, to proficiently benefit from heterojunction construction (Ref. 8, 19, 30).

In our recent works, we have utilized hybrid vapor-liquid phase assisted preparation route to obtain composite systems in which gCN deposits, obtained by electrophoretic deposition (EPD), were functionalized by sputtering with metal/metal oxide nanoparticles to yield advanced photoelectrocatalysts (Ref. 32-36). Based on these results, in the present work we focus on Fe_2O_3-gCN nanocomposites fabricated by an alternative route, *i.e.* the plasma assisted-chemical vapor deposition (PA-CVD) of Fe_2O_3 on fluorine-doped tin oxide (FTO) substrates and the subsequent dispersion of gCN in low amounts *via* EPD. The last synthetic step was carried out utilizing two different kinds of gCN powders, obtained from melamine [gCN(M)] and melamine + cyanuric acid [gCN(CM)], as precursors, with the aim of

[a)] Authors to whom correspondence should be addressed. E-mail: mattia.benedet@phd.unipd.it (M.B.); davide.barreca@unipd.it (D.B.).

manufacturing systems characterized by a different defectivity (Ref. 33). As a part of a comprehensive research work aimed at the design, synthesis and characterization of Fe_2O_3-gCN photoelectrodes for solar-activated water splitting, in this contribution we present a detailed X-ray photoelectron spectroscopy (XPS) analysis of the main photoelectron peaks (C 1s, O 1s, Fe 2p, and N 1s) for bare Fe_2O_3, Fe_2O_3-gCN(M), and Fe_2O_3-gCN(CM) nanocomposite systems. The obtained results provide evidence for the formation of systems in which iron(III) oxide and graphitic carbon nitride maintain their chemical identity. Nevertheless, a careful analysis of binding energy (BE) values evidences the formation of type-II heterojunctions yielding charge carrier separation at Fe_2O_3/gCN interface, more effective in the case of gCN(CM), which was characterized by a higher defect content than gCN(M). These results may offer a valuable comparison for future XPS studies of analogous materials developed by various procedures for different technological end-uses.

SPECIMEN DESCRIPTION (ACCESSION # 01865)

Host Material: Fe_2O_3

CAS Registry #: 1309-37-1

Host Material Characteristics: homogeneous; solid; polycrystalline; semiconductor; inorganic compound; Thin Film

Chemical Name: Iron(III) oxide

Source: sample fabricated by PA-CVD of Fe_2O_3 on a FTO substrate, followed by thermal treatment in air at 520°C for 3 h.

Host Composition: C, O, Fe

Form: Supported thin film

Structure: The system structure and morphology were investigated by means of X-ray diffraction (XRD) and field emission-scanning electron microscopy (FE-SEM), respectively. The XRD pattern was characterized by the presence of peaks at 24.1, 33.2, 35.5, 41.0, and 49.5°, corresponding to the (012), (104), (110), (113), and (024) crystallographic planes of α-Fe_2O_3 (*hematite*) (Ref. 37), the most thermodynamically stable iron(III) oxide polymorph under ordinary conditions (Refs. 3, 28, 38). No other signals could be clearly identified, indicating the formation of phase-pure systems. FE-SEM images evidenced the formation of elongated structures assembled to yield porous systems with a high active area, an amenable feature for photo(electro)catalytic applications. The average deposit thickness was estimated to be 450 nm.

History & Significance: Fe_2O_3 deposition was carried out on a pre-cleaned FTO-coated glass slide (Aldrich, ≈7 Ω/sq; FTO thickness ≈ 600 nm) by means of a custom-built two-electrode plasmochemical apparatus equipped with a 13.56 MHz radio frequency (RF) generator. $Fe(tfa)_2TMEDA$ (tfa = 1,1,1,-trifluoro-2,4-pentanedionate; TMEDA = *N*,*N*,*N'*,*N'*-tetramethylethylenediamine) (Ref. 39) was used as the iron precursor. The compound, placed in an external glass reservoir, was vaporized at 85°C by means of an external oil bath, and its vapors were transported into the reaction chamber by means of an Ar flow [rate = 60 standard cubic centimeters per minute (sccm)]. The connection lines were heated at 150°C in order to prevent detrimental precursor condensation events. Additional Ar and O_2 flows (rates = 15 and 20 sccm, respectively) were introduced into the reactor through separate inlets. After preliminary optimization experiments, the following settings were adopted: total pressure = 1.0 mbar; growth temperature = 400°C; duration = 90 min; RF-power = 20 W. The obtained specimen was annealed in air at 520°C for 3 h.

As Received Condition: as grown

Analyzed Region: same as host material

Ex Situ Preparation/Mounting: Sample fixed with a copper tape on a grounded sample holder and introduced into the analysis chamber through a fast entry lock system.

In Situ Preparation: None

Charge Control: No flood gun was used.

Temp. During Analysis: 300 K

Pressure During Analysis: 2×10^{-8} Pa

Pre-analysis Beam Exposure: 120 s.

SPECIMEN DESCRIPTION (ACCESSION # 01866)

Host Material: Fe_2O_3-gCN(M)

CAS Registry #: unknown

Host Material Characteristics: homogeneous; solid; polycrystalline; semiconductor; composite; Thin Film

Chemical Name: Iron(III) oxide-graphitic carbon nitride

Source: sample prepared by PA-CVD of Fe_2O_3 on a FTO substrate, followed by functionalization with gCN(M) by EPD and thermal treatment in air at 520°C for 3 h.

Host Composition: C, N, O, Fe

Form: Supported nanocomposite thin film

Structure: XRD analysis yielded a diffraction pattern very similar to the one of the previous accession and no reflections related to gCN presence could be unambiguously assigned. This result was traced back to the very low amount and high dispersion of gCN into the hosting Fe_2O_3 deposit (that did not undergo any major morphological alteration), as also confirmed by FE-SEM and transmission electron microscopy (TEM) characterization.

History & Significance: For the obtainment of the present specimen, PA-CVD conditions for Fe_2O_3 deposition were the same adopted for the previous accession. Afterwards, functionalization of Fe_2O_3 with gCN(M) was performed by EPD. The gCN(M) powders were obtained (Ref. 33) from pre-grinded melamine, heated in Ar for 30 min at 100°C, 400°C for 2 h, and finally at 550°C for 4 h. EPD depositions were carried out from gCN and I_2 suspensions in acetone (Ref. 40), using FTO-supported Fe_2O_3 (see the previous accession) as cathode, carbon paper as anode, and the following pre-optimized conditions: applied potential = 10 V; duration = 20 s. After solvent evaporation, the sample was annealed in air for 3 h at 520°C.

As Received Condition: as grown

Analyzed Region: same as host material

Ex Situ Preparation/Mounting: Sample fixed with a copper tape on a grounded sample holder and introduced into the analysis chamber through a fast entry lock system.

In Situ Preparation: None

Charge Control: No flood gun was used.

Temp. During Analysis: 300 K

Pressure During Analysis: 2×10^{-8} Pa

Pre-analysis Beam Exposure: 120 s.

SPECIMEN DESCRIPTION (ACCESSION # 01867)

Host Material: Fe_2O_3-gCN(CM)

CAS Registry #: unknown

Host Material Characteristics: homogeneous; solid; polycrystalline; semiconductor; composite; Thin Film

Chemical Name: Iron(III) oxide-graphitic carbon nitride

Source: sample prepared by PA-CVD of Fe_2O_3 on a FTO substrate, followed by functionalization with gCN(CM) by EPD and thermal treatment in air at 520°C for 3 h

Host Composition: C, N, O, Fe

Form: Supported nanocomposite thin film

Structure: The system structural and morphological features, as deduced by XRD and TEM characterization, turned out to be similar to those of sample accession # 01866.

History & Significance: The target sample was fabricated using the procedure already described for accession # 01866, adopting the same synthesis and processing conditions. The only difference was the use of gCN(CM) precursor powders, which were obtained from melamine (M) and cyanuric acid (C) separately dissolved under sonication in dimethylsulfoxide (Ref. 41). After heating at 60°C, the C-containing solution was introduced dropwise into the M-containing one under stirring. The obtained suspension was filtered after 10 min, and the recovered product, after washing with ethanol, was dried in Ar at 50°C for 3 h, and subsequently annealed at 500°C for 2.5 h, yielding light brown powders.

As Received Condition: as grown

Analyzed Region: same as host material

Ex Situ Preparation/Mounting: Sample fixed with a copper tape on a grounded sample holder and introduced into the analysis chamber through a fast entry lock system.

In Situ Preparation: None

Charge Control: No flood gun was used.

Temp. During Analysis: 300 K

Pressure During Analysis: 2×10^{-8} Pa

Pre-analysis Beam Exposure: 120 s.

INSTRUMENT DESCRIPTION

Manufacturer and Model: PHI 5000 Versaprobe

Analyzer Type: spherical sector

Detector: Channeltron

Number of Detector Elements: 16

INSTRUMENT PARAMETERS COMMON TO ALL SPECTRA

■*Spectrometer*

Analyzer Mode: constant pass energy

Throughput ($T=E^N$): N = 0

Excitation Source Window: 2.4 micron Al window

Excitation Source: Al Ka monochromatic

Source Energy: 1486.6 eV

Source Strength: 100 W

Source Beam Size: 200 μm × 200 μm

Signal Mode: multichannel direct

■*Geometry*

Incident Angle: 0˚

Source-to-Analyzer Angle: 45˚

Emission Angle: 45˚

Specimen Azimuthal Angle: 0˚

Acceptance Angle from Analyzer Axis: 0˚

Analyzer Angular Acceptance Width: 25˚ × 25˚

■*Ion Gun*

Manufacturer and Model: PHI FIG-5CE part no. 710620 Rev. A

Energy: 2000 eV

Current: 4 microA/mm2

Current Measurement Method: Faraday cup

Sputtering Species: Ar^+

Spot Size (unrastered): 600 μm

Raster Size: 1000 μm x 1000 μm

Incident Angle: 36˚

Polar Angle: 45˚

Azimuthal Angle: 111˚

Comment: differentially pumped ion gun

DATA ANALYSIS METHOD

Energy Scale Correction: None

Recommended Energy Scale Shift: 0 eV for all specimens

Peak Shape and Background Method: After a Shirley-type background subtraction (Ref. 42), BE and full width at half maximum (FWHM) values were evaluated by least-squares fitting adopting Gaussian/Lorentzian sum functions.

Quantitation Method: Atomic concentrations were calculated by peak area integration, using sensitivity factors provided by PHI.

ACKNOWLEDGMENTS

CNR (Progetti di Ricerca @CNR – avviso 2020 - ASSIST), Padova University (P-DiSC#04BIRD2020-UNIPD EUREKA, DOR 2020-2023), INSTM Consortium (INSTM21PDGASPAROTTO - NANO^{MAT}, INSTM21PDBARMAC - ATENA), and PRIN 2022474YE8 (SCI-TROPHY project) assisted financially the work. The authors are also grateful to Dr. Alessandra Banzato for experimental assistance.

AUTHOR DECLARATIONS

Conflicts of Interest

The authors have no conflicts to disclose.

Author contributions

Mattia Benedet: Conceptualization (lead); Data curation (equal); Methodology (lead); Validation (equal); Visualization (equal); Writing – review & editing (equal). **Davide Barreca:** Conceptualization (equal); Formal analysis (equal); Funding acquisition (equal); Resources (equal); Writing – review & editing (lead). **Gian Andrea Rizzi:** Data curation (equal); Investigation (equal); Software (equal); Supervision (equal); Visualization (equal). **Alberto Gasparotto:** Formal analysis (lead); Investigation (lead); Methodology (equal); Validation (lead); Writing – original draft (lead). **Jan-Lucas Wree:** Data curation (equal); Methodology (equal); Formal analysis (equal); Validation (equal); Visualization (equal); Writing – review & editing (equal). **Anjana Devi:** Methodology (equal); Formal analysis (equal); Visualization (equal); Writing – review & editing (equal). **Chiara Maccato:** Formal analysis (equal); Funding acquisition (lead); Methodology (equal); Supervision (equal); Visualization (lead); Writing – review & editing (lead).

DATA AVAILABILITY STATEMENT

The data that support the findings of this study are available within the article and its supplementary material.

REFERENCES

1. D. Barreca, G. Carraro, A. Gasparotto, C. Maccato, M. E. A. Warwick, K. Kaunisto, C. Sada, S. Turner, Y. Gönüllü, T.-P. Ruoko, L. Borgese, E. Bontempi, G. Van Tendeloo, H. Lemmetyinen, and S. Mathur, Adv. Mater. Interfaces **2**, 1500313 (2015).
2. S. A. Hassanzadeh-Tabrizi, C.-C. Nguyen, and T.-O. Do, Appl. Surf. Sci. **489**, 741 (2019).
3. P. Sharma, J.-W. Jang, and J. S. Lee, ChemCatChem **11**, 157 (2019).
4. F. Wang, R. Ou, H. Yu, Y. Lu, J. Qu, S. Zhu, L. Zhang, and M. Huo, Appl. Surf. Sci. **565**, 150597 (2021).
5. J. K. George, A. Bhagat, B. Bhaduri, and N. Verma, Catal. Lett. **153**, 419 (2023).
6. A. Mettenbörger, Y. Gönüllü, T. Fischer, T. Heisig, A. Sasinska, C. Maccato, G. Carraro, C. Sada, D. Barreca, L. Mayrhofer, M. Moseler, A. Held, and S. Mathur, Nano Energy **19**, 415 (2016).
7. Y. Liu, Y.-X. Yu, and W.-D. Zhang, Int. J. Hydrogen Energy **39**, 9105 (2014).
8. N. A. Arzaee, M. F. Mohamad Noh, N. S. H. Mohd Ita, N. A. Mohamed, S. N. F. Mohd Nasir, I. N. Nawas Mumthas, A. F. Ismail, and M. A. Mat Teridi, Dalton Trans. **49**, 11317 (2020).
9. K. C. Christoforidis, T. Montini, E. Bontempi, S. Zafeiratos, J. J. D. Jaén, and P. Fornasiero, Appl. Catal., B **187**, 171 (2016).
10. G. Carraro, C. Maccato, A. Gasparotto, K. Kaunisto, C. Sada, and D. Barreca, Plasma Processes Polym. **13**, 191 (2016).
11. Y. Liu, F.-Y. Su, Y.-X. Yu, and W.-D. Zhang, Int. J. Hydrogen Energy **41**, 7270 (2016).
12. S. Kang, J. Jang, R. C. Pawar, S.-H. Ahn, and C. S. Lee, RSC Adv. **8**, 33600 (2018).
13. C. Kim, K. M. Cho, K. Park, K. H. Kim, I. Gereige, and H.-T. Jung, ChemPlusChem **85**, 169 (2020).
14. J. Wang, X. Zuo, W. Cai, J. Sun, X. Ge, and H. Zhao, Dalton Trans. **47**, 15382 (2018).
15. X. Zou, Z. Sun, and Y. H. Hu, J. Mater. Chem. A **8**, 21474 (2020).
16. Y. Shen, Q. Han, J. Hu, W. Gao, L. Wang, L. Yang, C. Gao, Q. Shen, C. Wu, X. Wang, X. Zhou, Y. Zhou, and Z. Zou, ACS Appl. Energy Mater. **3**, 6561 (2020).
17. S.-W. Lv, J.-M. Liu, N. Zhao, C.-Y. Li, F.-E. Yang, Z.-H. Wang, and S. Wang, Sep. Purif. Technol. **253**, 117413 (2020).
18. Y. Geng, D. Chen, N. Li, Q. Xu, H. Li, J. He, and J. Lu, Appl. Catal., B **280**, 119409 (2021).
19. B. Zhu, B. Cheng, J. Fan, W. Ho, and J. Yu, Small Struct. **2**, 2100086 (2021).
20. W. Xiong, F. Huang, and R.-Q. Zhang, Sustainable Energy Fuels **4**, 485 (2020).
21. J. Theerthagiri, R. A. Senthil, A. Priya, J. Madhavan, R. J. V. Michael, and M. Ashokkumar, RSC Adv. **4**, 38222 (2014).
22. S. Xiong, X. Liu, X. Zhu, G. Liang, Z. Jiang, B. Cui, and J. Bai, Ecotoxicol. Environ. Saf. **208**, 111519 (2021).
23. X. Liu, A. Jin, Y. Jia, J. Jiang, N. Hu, and X. Chen, RSC Adv. **5**, 92033 (2015).
24. Y. Liu, X. Xu, A. Li, Z. Si, X. Wu, R. Ran, and D. Weng, Catal. Commun. **157**, 106327 (2021).
25. Z. Pan, G. Zhang, and X. Wang, Angew. Chem. Int. Ed. **58**, 7102 (2019).
26. Y. Li, X. Wei, X. Yan, J. Cai, A. Zhou, M. Yang, and K. Liu, Phys. Chem. Chem. Phys **18**, 10255 (2016).
27. S. Lee, and J.-W. Park, Sustainability **12**, 2866 (2020).
28. L. Zhang, X. Zhang, C. Wei, F. Wang, H. Wang, and Z. Bian, Chem. Eng. J. **435**, 134873 (2022).
29. Z. Jiang, W. Wan, H. Li, S. Yuan, H. Zhao, and P. K. Wong, Adv. Mater. **30**, 1706108 (2018).
30. Q. Xu, B. Zhu, C. Jiang, B. Cheng, and J. Yu, Sol. RRL **2**, 1800006 (2018).
31. L. Bigiani, D. Barreca, A. Gasparotto, T. Andreu, J. Verbeeck, C. Sada, E. Modin, O. I. Lebedev, J. R. Morante, and C. Maccato, Appl. Catal., B **284**, 119684 (2021).
32. M. Benedet, G. A. Rizzi, A. Gasparotto, N. Gauquelin, A. Orekhov, J. Verbeeck, C. Maccato, and D. Barreca, Appl. Surf. Sci. **618**, 156652 (2023).
33. M. Benedet, G. Andrea Rizzi, A. Gasparotto, O. I. Lebedev, L. Girardi, C. Maccato, and D. Barreca, Chem. Eng. J. **448**, 137645 (2022).
34. M. Benedet, A. Gasparotto, G. A. Rizzi, D. Barreca, and C. Maccato, Surf. Sci. Spectra **29**, 024001 (2022).
35. M. Benedet, G. A. Rizzi, D. Barreca, A. Gasparotto, and C. Maccato, Surf. Sci. Spectra **30**, 014004 (2023).
36. S. Benedoue, M. Benedet, A. Gasparotto, N. Gauquelin, A. Orekhov, J. Verbeeck, R. Seraglia, G. Pagot, G. A. Rizzi, V. Balzano, L. Gavioli, V. D. Noto, D. Barreca, and C. Maccato, Nanomaterials **13**, 1035 (2023).
37. Pattern No. 033-0664, JCPDS (2000).
38. Y. Kumar, R. Kumar, P. Raizada, A. A. P. Khan, A. Singh, Q. V. Le, V.-H. Nguyen, R. Selvasembian, S. Thakur, and P. Singh, J. Environ. Chem. Eng. **10**, 107427 (2022).
39. D. Barreca, L. Bigiani, M. Klotzsche, A. Gasparotto, R. Seraglia, C. Jandl, A. Pöthig, E. Fois, L. Vanin, G. Tabacchi, M. Roverso, S. Bogialli, E. Callone, S. Dirè, and C. Maccato, Mater. Chem. Phys. **277**, 125534 (2022).
40. S. Zhang, J. Yan, S. Yang, Y. Xu, X. Cai, X. Li, X. Zhang, F. Peng, and Y. Fang, Chin. J. Catal. **38**, 365 (2017).
41. Y.-S. Jun, E. Z. Lee, X. Wang, W. H. Hong, G. D. Stucky, and A. Thomas, Adv. Funct. Mater. **23**, 3661 (2013).
42. D. A. Shirley, Phys. Rev. B **5**, 4709 (1972).
43. M. Guo, M. Chen, J. Xu, C. Wang, and L. Wang, Chem. Eng. J. **461**, 142046 (2023).
44. J. F. Moulder, W. F. Stickle, P. E. Sobol, and K. D. Bomben, *Handbook of X-ray Photoelectron Spectroscopy* (Perkin Elmer Corporation, Eden Prairie, MN, USA, 1992).
45. http://srdata.nist.gov/xps.
46. R. Khurram, Z. U. Nisa, A. Javed, Z. Wang, and M. A. Hussien, Molecules **27**, 1442 (2022).

47. Y. Wu, J. Ward-Bond, D. Li, S. Zhang, J. Shi, and Z. Jiang, ACS Catal. **8**, 5664 (2018).
48. C. Maccato, L. Bigiani, L. Girardi, A. Gasparotto, O. I. Lebedev, E. Modin, D. Barreca, and G. A. Rizzi, Adv. Mater. Interfaces **8**, 2100763 (2021).
49. Y. Li, S. Zhu, Y. Liang, Z. Li, S. Wu, C. Chang, S. Luo, and Z. Cui, Mater. Des. **196**, 109191 (2020).

SPECTRAL FEATURES TABLE							
Spectrum ID #	**Element/ Transition**	**Peak Energy (eV)**	**Peak Width FWHM (eV)**	**Peak Area (eV x cts/s)**	**Sensitivity Factor**	**Concentration (at. %)**	**Peak Assignment**
01865-02[a]	C 1s	284.8	1.5	6563.83	19.641	21.00	Adventitious contamination
01865-02[a]	C 1s	288.0	2.0	869.73	19.641	2.78	Surface-chemisorbed carbonates
01865-03[b]	O 1s	529.9	1.2	33207.18	50.082	42.29	Lattice O in Fe_2O_3
01865-03[b]	O 1s	531.6	1.8	8146.72	50.082	10.38	Surface-chemisorbed hydroxyls/carbonates
01865-04[c]	Fe 2p	…	…	83100.83	231.014	23.55	Fe(III) in Fe_2O_3
01865-04	Fe $2p_{3/2}$	711.2	2.7	…	…	…	Fe(III) in Fe_2O_3
01865-04	Fe $2p_{1/2}$	724.7	2.8	…	…	…	Fe(III) in Fe_2O_3
01866-02[a]	C 1s	284.8	1.5	6720.92	19.641	21.01	Adventitious contamination
01866-02[a]	C 1s	286.4	1.8	593.49	19.641	1.86	C in C-NH_x (x = 1,2) groups located on gCN heptazine ring edges
01866-02[a]	C 1s	288.4	1.6	705.78	19.641	2.21	Surface-chemisorbed carbonates and N=C-N C atoms in the framework of gCN aromatic rings
01866-03[d]	N 1s	398.8	1.8	61.04	33.673	0.11	Bi-coordinated N atoms (C=N-C) in gCN
01866-03[d]	N 1s	400.1	1.8	58.38	33.673	0.10	Tri-coordinated N atoms [N-$(C)_3$] in gCN
01866-03[d]	N 1s	401.3	1.6	13.27	33.673	0.03	Uncondensed NH_x groups (x = 1,2)
01866-04[b]	O 1s	529.7	1.2	35351.03	50.082	43.32	Lattice O in Fe_2O_3
01866-04[b]	O 1s	531.6	1.8	5850.64	50.082	7.17	Surface-chemisorbed hydroxyls/carbonates
01866-05[c]	Fe 2p	…	…	91098.76	231.014	24.20	Fe(III) in Fe_2O_3
01866-05	Fe $2p_{3/2}$	711.0	2.9	…	…	…	Fe(III) in Fe_2O_3
01866-05	Fe $2p_{1/2}$	724.5	3.0	…	…	…	Fe(III) in Fe_2O_3
01867-02[a]	C 1s	284.8	1.5	5968.52	19.641	19.75	Adventitious contamination
01867-02[a]	C 1s	286.5	1.9	561.33	19.641	1.86	C in C-NH_x (x = 1,2) groups located on gCN heptazine ring edges
01867-02[a]	C 1s	288.5	1.7	575.54	19.641	1.90	Surface-chemisorbed carbonates and N=C-N C atoms in the framework of gCN aromatic rings
01867-03[d]	N 1s	398.9	1.5	96.90	33.673	0.19	Bi-coordinated N atoms (C=N-C) in gCN
01867-03[d]	N 1s	400.2	1.6	90.91	33.673	0.17	Tri-coordinated N atoms [N-$(C)_3$] in gCN
01867-03[d]	N 1s	401.4	1.8	61.94	33.673	0.12	Uncondensed NH_x groups (x = 1,2)
01867-04[b]	O 1s	529.6	1.2	33143.24	50.082	43.01	Lattice O in Fe_2O_3
01867-04[b]	O 1s	531.6	1.7	7324.70	50.082	9.50	Surface-chemisorbed hydroxyls/carbonates
01867-05[c]	Fe 2p	…	…	83569.95	231.014	23.50	Fe(III) in Fe_2O_3
01867-05	Fe $2p_{3/2}$	710.9	2.9	…	…	…	Fe(III) in Fe_2O_3
01867-05	Fe $2p_{1/2}$	724.4	3.0	…	…	…	Fe(III) in Fe_2O_3

[a] The sensitivity factor is referred to the whole C 1s signal.
[b] The sensitivity factor is referred to the whole O 1s signal.
[c] The sensitivity factor, peak area, and concentration are referred to the whole Fe 2p signal.
[d] The sensitivity factor is referred to the whole N 1s signal.

Footnote to Spectra 01865-02, 01866-02 and 01867-02: In the case of specimen accession # 01865, the C 1s photoelectron peaks was fitted by means of two bands: the principal one, at 284.8 eV, attributable to adventitious contamination (Refs. 7, 20, 33-35, 43), and a second minor one at 288.0 eV, related to surface chemisorbed carbonates (Refs. 6, 44, 45). As concerns samples accessions # 01866 and # 01867, three different components were identified. Beside the main one at 284.8 eV (I), the signal at 286.4-286.5 (II) was attributed to C-NH_x (x = 1, 2) groups located on gCN heptazine ring edges (Refs. 2, 14, 32-34, 36, 43). The occurrence of these amino groups, that should be absent in a fully condensed carbon nitride structure, can favorably influence the anchoring of carbon nitride to the underlying Fe_2O_3 deposits. Beside improving material operational stability, an important pre-requisite for the use of these systems as photoelectrocatalysts, this issue, in turn, can improve charge transfer processes from carbon nitride to iron

oxide (Refs. 15) (see below). Finally, the higher BE component (III, 288.4-288.5 eV) could be assigned not only to surface chemisorbed carbonates arising from air exposure (see the data for sample accession # 01865), but also to N-C=N carbon atoms in the framework of graphitic carbon nitride (Refs. 4, 18, 27, 43, 46, 47). It is worthwhile noticing that the energy positions of (II) and (III) underwent a blue shift in comparison to bare gCN (Refs. 25-27, 34, 35, 46, 48, 49), corresponding to +0.2 and +0.3 eV for sample accessions # 01866 and # 01867, respectively. This issue, in line with the experimental results obtained by the analysis of N 1s, O 1s, and Fe 2p photoelectron peaks (see comments to the following accessions), suggested the formation of a type-II heterojunction at Fe_2O_3/gCN interface, according to which photoexcited electrons and holes are accumulated in Fe_2O_3 conduction band and gCN valence band, respectively (Refs. 4, 15, 21, 23, 31, 33, 46). This phenomenon results in a suppressed recombination of photoproduced charge carriers, favorably boosting catalytic activity. The more marked shift observed in the case of sample accession # 01867 indicates the occurrence of a more efficient junction in comparison to # 01866, anticipating thus improved functional performances for this specimen.

Footnote to Spectra 01865-03, 01866-04 and 01867-04: For all the analyzed specimens, fitting the O 1s signals yielded two different components. The main one (BE = 529.9-529.6 eV) was assigned to lattice oxygen in Fe_2O_3 network (Refs. 5, 18, 25, 28, 30, 47), whereas the one at higher BE (531.6 eV) was ascribed to -OH groups chemisorbed on oxygen defects (Refs. 4, 8, 14, 16, 29, 46). The occurrence of the latter can be beneficial in view of photoelectrocatalytic applications (Refs. 31, 48). The lattice O band was progressively shifted to lower BEs upon going from sample accession # 01865 (529.9 eV), to # 01866 (529.7 eV), to # 01867 (529.6 eV). This shift, occurring in the opposite direction of the one experienced by C 1s (II) and (III) components (see Footnote to Spectra 01865-02, 01866-02 and 01867-02), supporting thus the above mentioned type-II heterojunction formation and related charge transfer mechanism.

Footnote to Spectra 01865-04, 01866-05 and 01867-05: The above charge transfer scheme is further supported by a detailed analysis of Fe 2p photoelectron peaks. As regards sample accession # 01865, the Fe 2p peak shape and position were in line with those reported for phase-pure Fe_2O_3 [BE($Fe2p_{3/2}$) = 711.2 eV; spin-orbit splitting = 13.5 eV] (Refs. 1, 8, 10, 29, 47-49). In comparison to bare iron oxide, specimen accessions # 01866 and 01867 showed a BE decrease of 0.2 eV and 0.3 eV, respectively. As already mentioned, this phenomenon could be explained basing on the formation of type-II heterojunctions (Ref. 12), with a gCN→Fe_2O_3 electron transfer (Ref. 4, 28) triggered by the close carbon nitride/iron(III) oxide contact in the target systems. The pronounced gCN→Fe_2O_3 electron transfer phenomenon for sample accession # 01867 results in an improved charge carrier separation.

Footnote to Spectra 01866-03 and 01867-03: For specimen accessions # 01866 and # 01867, the N 1s signal was fitted using three distinct components: (i), the predominant one (BE = 398.8-398.9 eV), assigned to nitrogen centers belonging to C=N-C groups (Refs. 2, 9, 24, 29, 36); (ii), located at 400.1-400.2 eV, attributed to tertiary N atoms [$(C)_3$-N] (Refs. 13, 18, 22, 30); (iii), at 401.3-401.4, related to nitrogen belonging to uncondensed amino groups C-NH_x (x = 1, 2) (Refs. 5, 14, 17, 22, 23, 47, 49). Due to the low overall nitrogen content in the analyzed specimens, the weak signal due to π-electron excitations in gCN heptazine rings, expected at BE ≈ 404. 2 eV (Refs. 34, 35), turned out to be undetectable. For sample accession # 01867, the relative weight of band (iii) underwent an appreciable increase in comparison to # 01866, indicating an enhancement of -NH_x-related defects content, an issue which is deemed to have a positive effect on material photoelectrocatalytic activity (Refs. 15, 32, 33, 36). In line with the data discussed in relation to the C 1s photopeaks (see Footnote to Spectra 01865-02, 01866-02 and 01867-02), components (i), (ii) and (iii) displayed an upward energy shift corresponding to +0.2 eV and +0.3 eV with respect to pure gCN (Refs. 23, 25-27, 34-36, 46, 48, 49). This result supported the occurrence of the aforementioned gCN→Fe_2O_3 electron transfer, more effective for sample accession # 01867.

ANALYZER CALIBRATION TABLE							
Spectrum ID #	**Element/ Transition**	**Peak Energy (eV)**	**Peak Width FWHM (eV)**	**Peak Area (eV x cts/s)**	**Sensitivity Factor**	**Concentration (at. %)**	**Peak Assignment**
…[a]	Au $4f_{7/2}$	84.0	0.8	32526	...	...	Au(0)
…[a]	Cu $2p_{3/2}$	932.7	0.9	39323	...	...	Cu(0)

[a] The peak was acquired after Ar^+ erosion at 2000 V for 8 min.

GUIDE TO FIGURES					
Spectrum (Accession) #	**Spectral Region**	**Voltage Shift***	**Multiplier**	**Baseline**	**Comment #**
01865-01	Survey	0	1	0	…
01865-02	C 1s	0	1	0	…
01865-03	O 1s	0	1	0	…
01865-04	Fe 2p	0	1	0	…
01866-01	Survey	0	1	0	…
01866-02	C 1s	0	1	0	…
01866-03	N 1s	0	1	0	…
01866-04	O 1s	0	1	0	…
01866-05	Fe 2p	0	1	0	…
01867-01	Survey	0	1	0	…
01867-02	C 1s	0	1	0	…
01867-03	N 1s	0	1	0	…
01867-04	O 1s	0	1	0	…
01867-05	Fe 2p	0	1	0	…

* Voltage shift of the archived (as measured) spectrum relative to the printed figure. The figure reflects the recommended energy scale correction due to a calibration correction, sample charging, flood gun, or other phenomena.

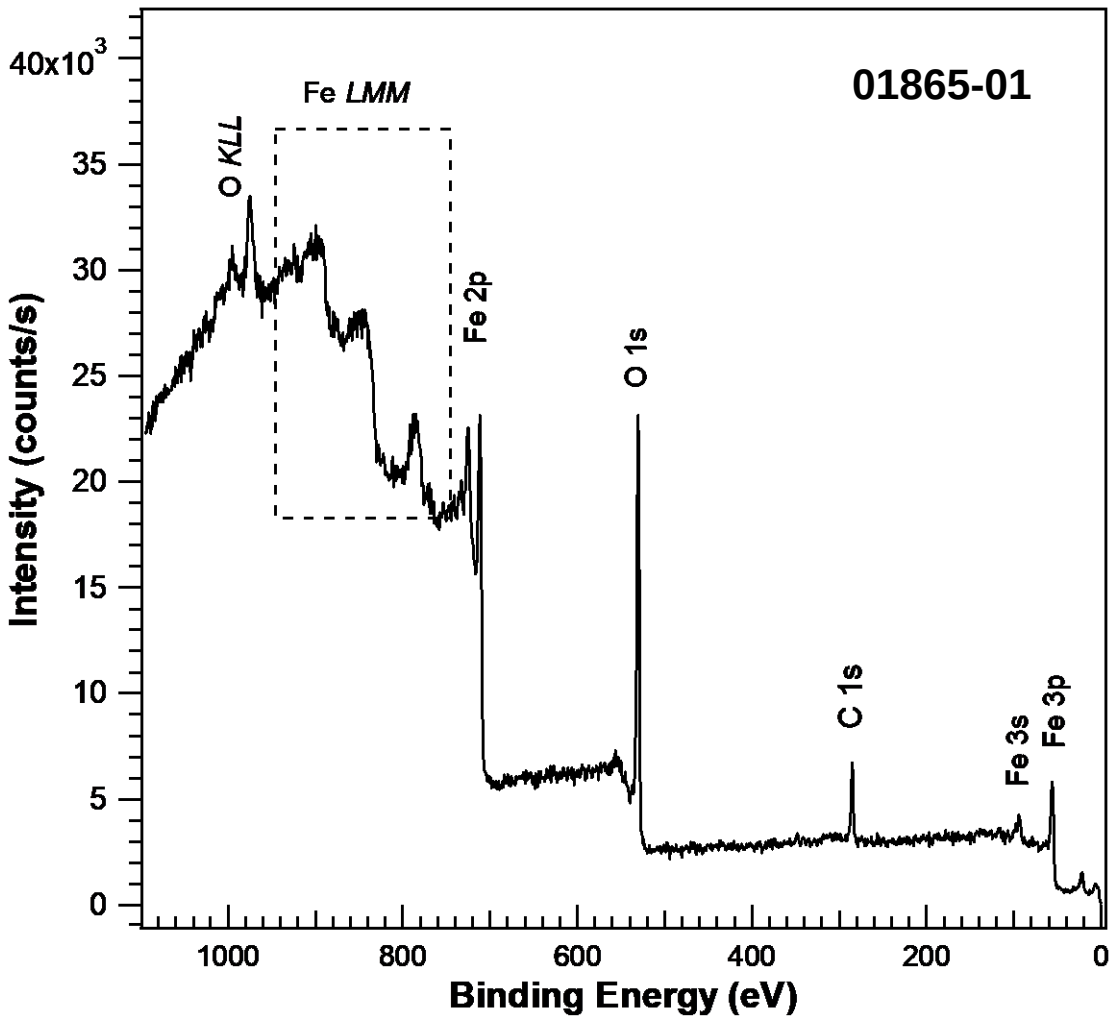

Publish in *Surface Science Spectra*: Yes X No ☐

Accession #	01865-01
Host Material	Fe_2O_3
Technique	XPS
Spectral Region	survey
Instrument	PHI 5000 Versaprobe
Excitation Source	Al Ka monochromatic
Source Energy	1486.6 eV
Source Strength	100 W
Source Size	0.2 mm x 0.2 mm
Analyzer Type	spherical sector analyzer
Incident Angle	0˚
Emission Angle	45˚
Analyzer Pass Energy	187.85 eV
Analyzer Resolution	1.9 eV
Total Signal Accumulation Time	220.2 s
Total Elapsed Time	242.2 s
Number of Scans	8
Effective Detector Width	1.9 eV

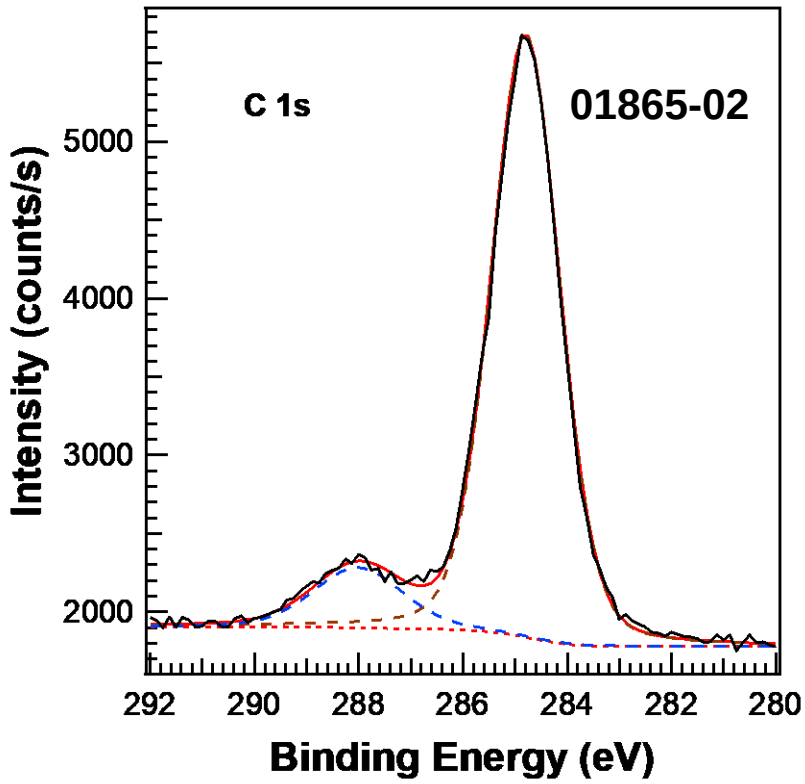

Publish in *SSS*: Yes X No ☐

- **Accession #:** 01865-02
- **Host Material:** Fe_2O_3
- **Technique:** XPS
- **Spectral Region:** C 1s

Instrument: PHI 5000 Versaprobe
Excitation Source: Al Ka monochromatic
Source Energy: 1486.6 eV
Source Strength: 100 W
Source Size: 0.2 mm x 0.2 mm
Analyzer Type: spherical sector
Incident Angle: 0˚
Emission Angle: 45˚
Analyzer Pass Energy 58.7 eV
Analyzer Resolution: 0.6 eV
Total Signal Accumulation Time: 444.0 s
Total Elapsed Time: 488.4 s

Number of Scans: 48
Enter source energy.
Effective Detector Width: 0.6 eV

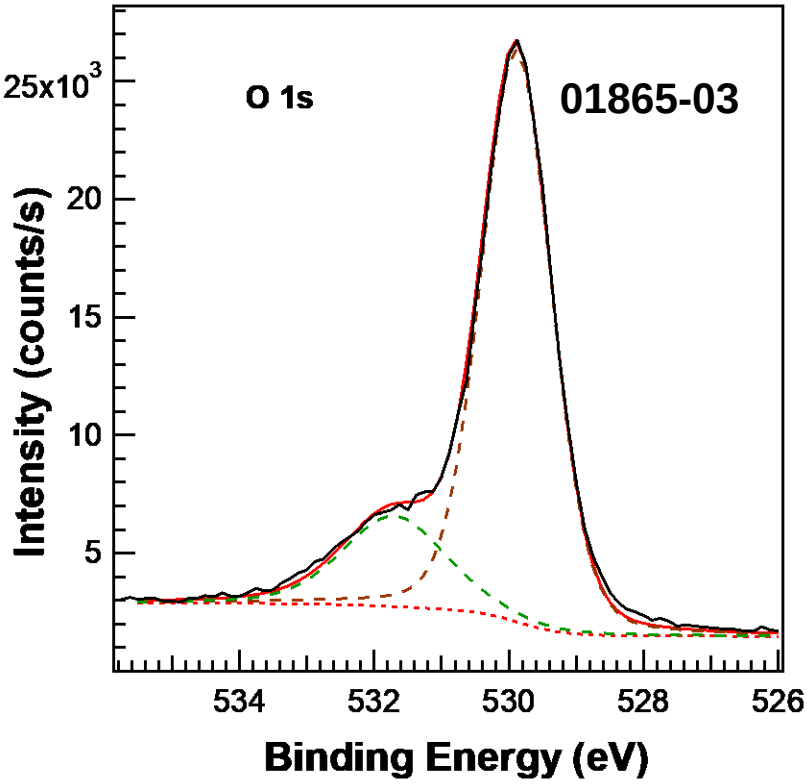

Publish in *SSS*: Yes X No ☐

- **Accession #:** 01865-03
- **Host Material:** Fe_2O_3
- **Technique:** XPS
- **Spectral Region:** O 1s

Instrument: PHI 5000 Versaprobe
Excitation Source: Al Ka monochromatic
Source Energy: 1486.6 eV
Source Strength: 100 W
Source Size: 0.2 mm x 0.2 mm
Analyzer Type: spherical sector
Incident Angle: 0˚
Emission Angle: 45˚
Analyzer Pass Energy 58.7 eV
Analyzer Resolution: 0.6 eV
Total Signal Accumulation Time: 70.8 s
Total Elapsed Time: 77.9 s

Number of Scans: 8

Effective Detector Width: 0.6 eV

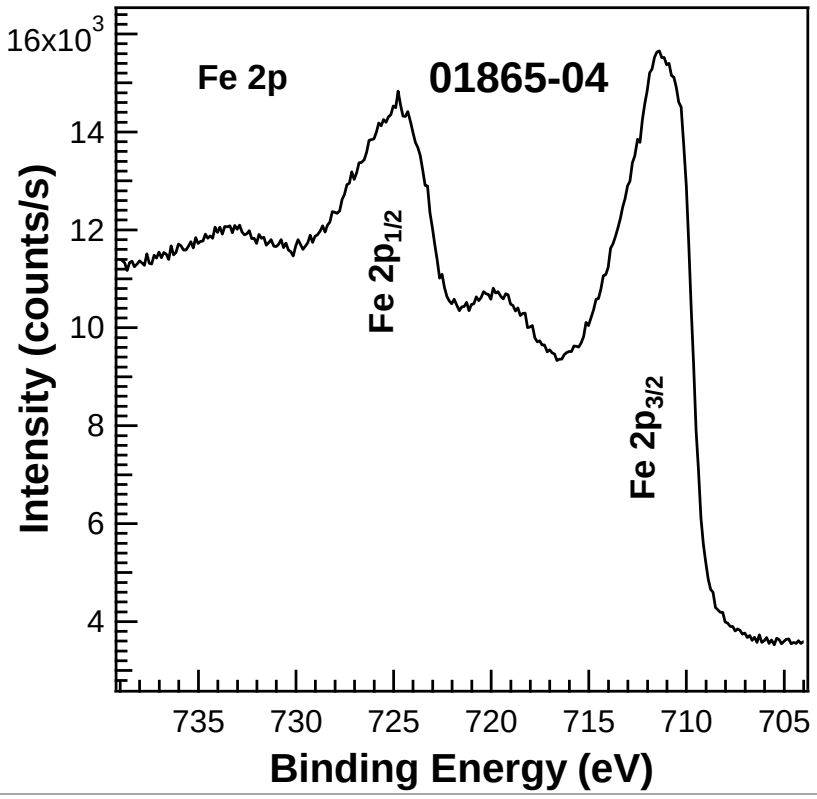

Publish in *SSS*: Yes X No ☐

- **Accession #:** 01865-04
- **Host Material:** Fe_2O_3
- **Technique:** XPS
- **Spectral Region:** Fe 2p

Instrument: PHI 5000 Versaprobe

Excitation Source: Al Ka monochromatic

Source Energy: 1486.6 eV

Source Strength: 100 W

Source Size: 0.2 mm x 0.2 mm

Analyzer Type: spherical sector

Incident Angle: 0˚

Emission Angle: 45˚

Analyzer Pass Energy 58.7 eV

Analyzer Resolution: 0.6 eV

Total Signal Accumulation Time: 513.6 s

Total Elapsed Time: 565.0 s

Number of Scans: 32

Effective Detector Width: 0.6 eV

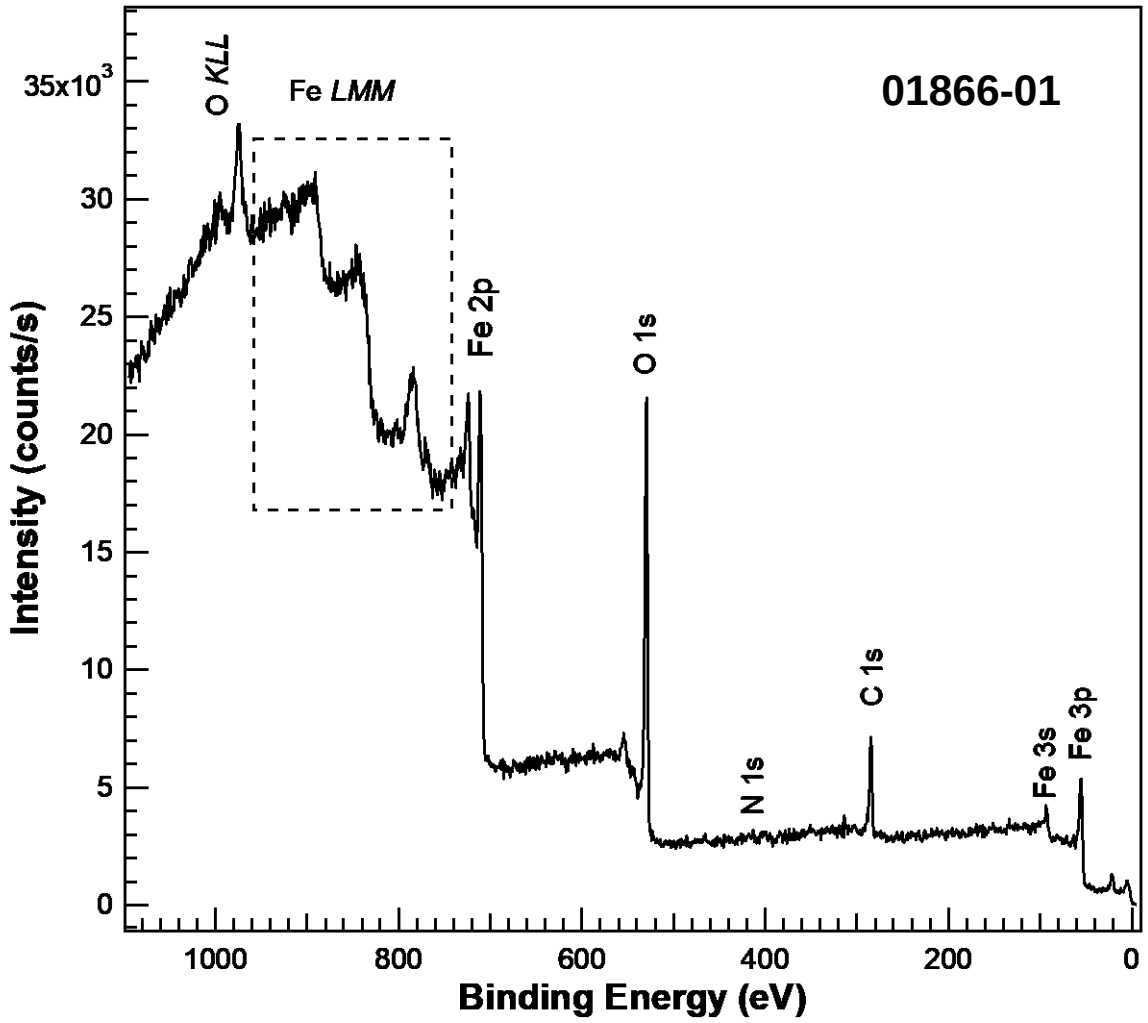

Publish in *Surface Science Spectra*: Yes ☒ No ☐

Accession #	01866-01
Host Material	Fe_2O_3-gCN(M)
Technique	XPS
Spectral Region	survey
Instrument	PHI 5000 Versaprobe
Excitation Source	Al Ka monochromatic
Source Energy	1486.6 eV
Source Strength	100 W
Source Size	0.2 mm x 0.2 mm
Analyzer Type	spherical sector analyzer
Incident Angle	0˚
Emission Angle	45˚
Analyzer Pass Energy	187.85 eV
Analyzer Resolution	1.9 eV
Total Signal Accumulation Time	220.2 s
Total Elapsed Time	242.2 s
Number of Scans	8
Effective Detector Width	1.9 eV

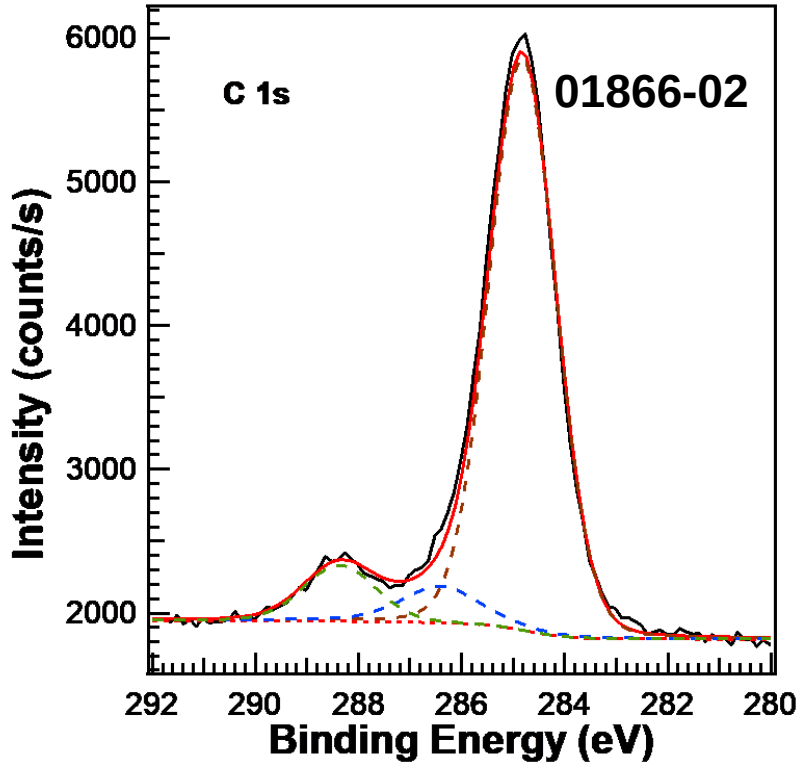

Publish in *SSS*: Yes X No ☐

- **Accession #:** 01866-02
- **Host Material:** Fe_2O_3-gCN(M)
- **Technique:** XPS
- **Spectral Region:** C 1s

Instrument: PHI 5000 Versaprobe
Excitation Source: Al Ka monochromatic
Source Energy: 1486.6 eV
Source Strength: 100 W
Source Size: 0.2 mm x 0.2 mm
Analyzer Type: spherical sector
Incident Angle: 0˚
Emission Angle: 45˚
Analyzer Pass Energy 58.7 eV
Analyzer Resolution: 0.6 eV
Total Signal Accumulation Time: 740.0 s
Total Elapsed Time: 814.0 s

Number of Scans: 80

Effective Detector Width: 0.6 eV

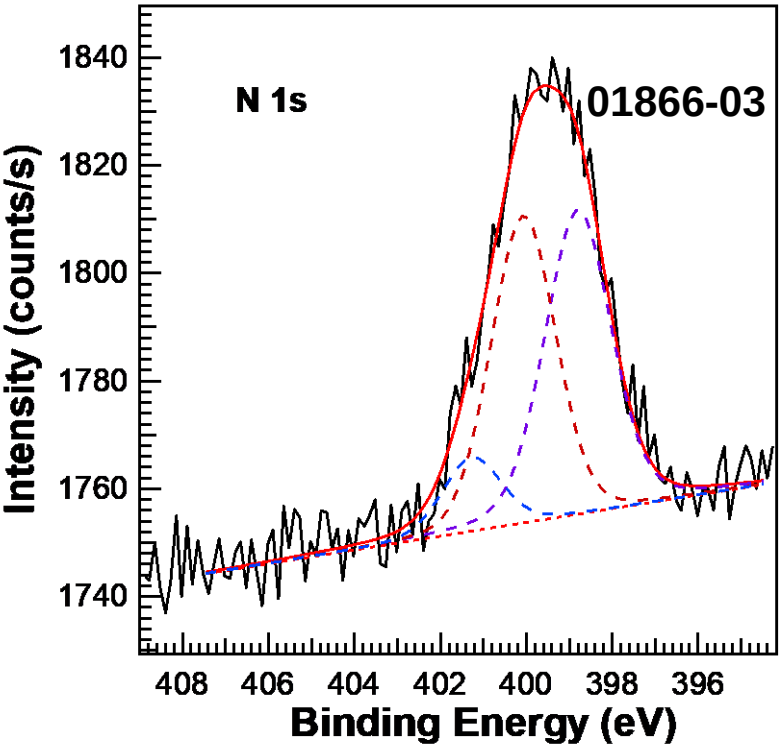

Publish in *SSS*: Yes X No ☐

- **Accession #:** 01866-03
- **Host Material:** Fe_2O_3-gCN(M)
- **Technique:** XPS
- **Spectral Region:** N 1s

Instrument: PHI 5000 Versaprobe
Excitation Source: Al Ka monochromatic
Source Energy: 1486.6 eV
Source Strength: 100 W
Source Size: 0.2 mm x 0.2 mm
Analyzer Type: spherical sector
Incident Angle: 0˚
Emission Angle: 45˚
Analyzer Pass Energy 58.7 eV
Analyzer Resolution: 0.6 eV
Total Signal Accumulation Time: 1888.0 s
Total Elapsed Time: 2076.8 s

Number of Scans: 320

Effective Detector Width: 0.6 eV

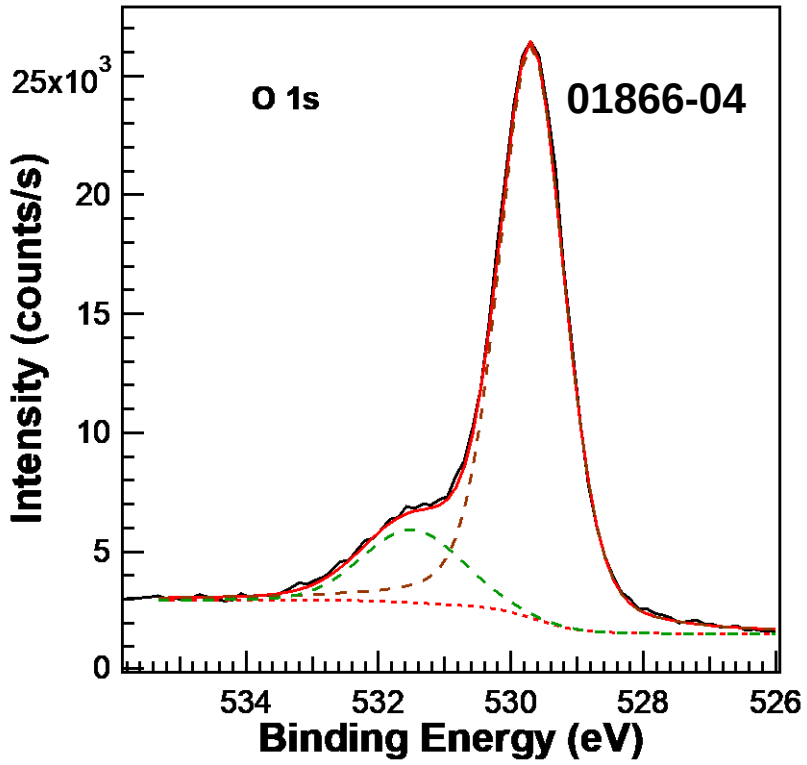

Publish in *SSS*: Yes X No ☐

- **Accession #:** 01866-04
- **Host Material:** Fe_2O_3-gCN(M)
- **Technique:** XPS
- **Spectral Region:** O 1s

Instrument: PHI 5000 Versaprobe
Excitation Source: Al Ka monochromatic
Source Energy: 1486.6 eV
Source Strength: 100 W
Source Size: 0.2 mm x 0.2 mm
Analyzer Type: spherical sector
Incident Angle: 0˚
Emission Angle: 45˚
Analyzer Pass Energy 58.7 eV
Analyzer Resolution: 0.6 eV
Total Signal Accumulation Time: 70.8 s
Total Elapsed Time: 77.9 s

Number of Scans: 8

Effective Detector Width: 0.6 eV

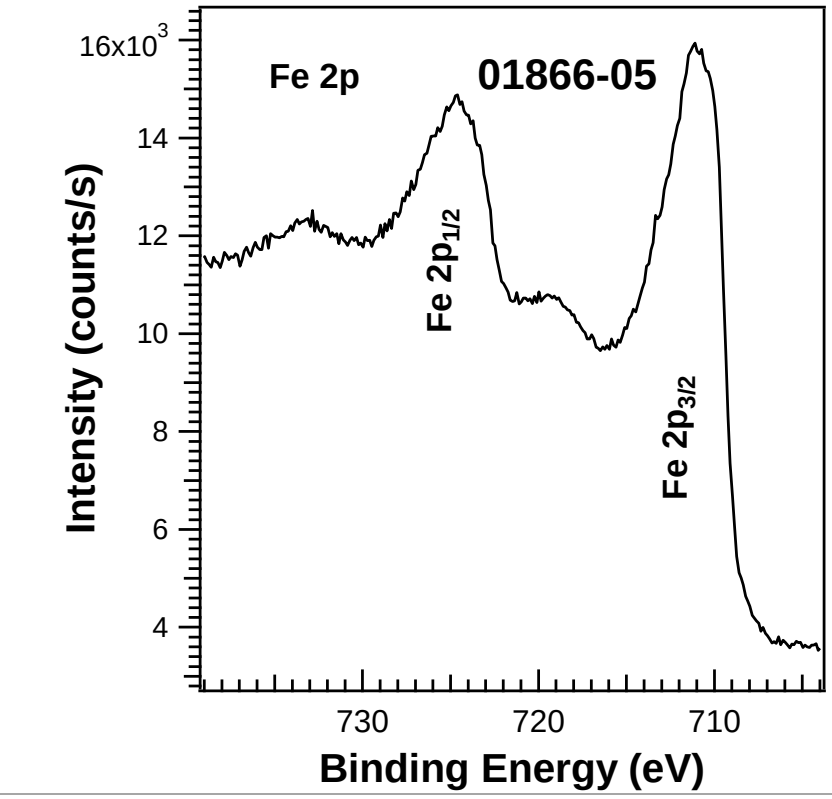

Publish in *SSS*: Yes X No ☐

- **Accession #:** 01866-05
- **Host Material:** Fe_2O_3-gCN(M)
- **Technique:** XPS
- **Spectral Region:** Fe 2p

Instrument: PHI 5000 Versaprobe
Excitation Source: Al Ka monochromatic
Source Energy: 1486.6 eV
Source Strength: 100 W
Source Size: 0.2 mm x 0.2 mm
Analyzer Type: spherical sector
Incident Angle: 0˚
Emission Angle: 45˚
Analyzer Pass Energy 58.7 eV
Analyzer Resolution: 0.6 eV
Total Signal Accumulation Time: 513.6 s
Total Elapsed Time: 565.0 s

Number of Scans: 32

Effective Detector Width: 0.6 eV

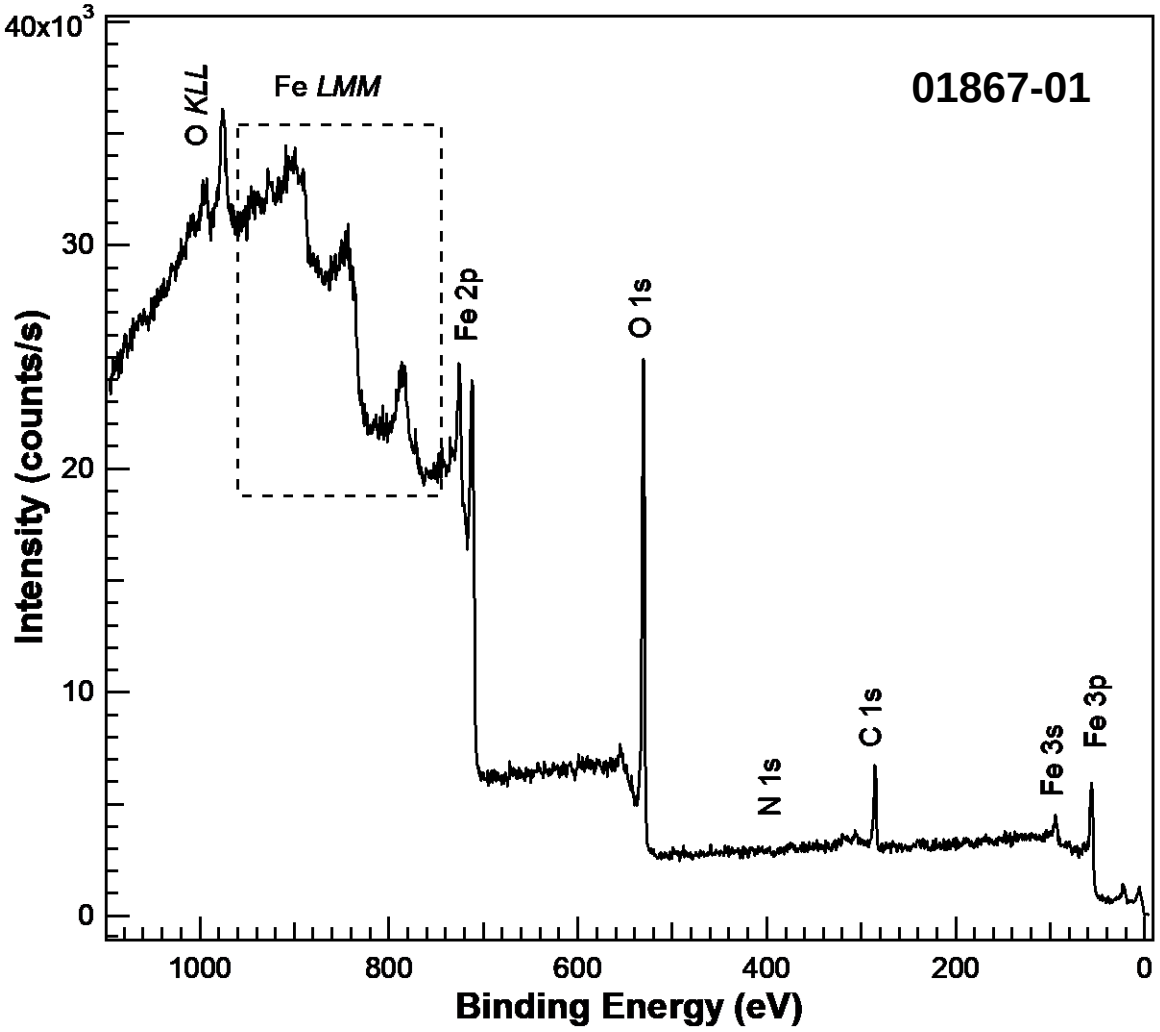

Publish in *Surface Science Spectra*: Yes X No ☐

Accession #	01867-01
Host Material	Fe_2O_3-gCN(CM)
Technique	XPS
Spectral Region	survey
Instrument	PHI 5000 Versaprobe
Excitation Source	Al Ka monochromatic
Source Energy	1486.6 eV
Source Strength	100 W
Source Size	0.2 mm x 0.2 mm
Analyzer Type	spherical sector analyzer
Incident Angle	0˚
Emission Angle	45˚
Analyzer Pass Energy	187.85 eV
Analyzer Resolution	1.9 eV
Total Signal Accumulation Time	220.2 s
Total Elapsed Time	242.2 s
Number of Scans	8
Effective Detector Width	1.9 eV

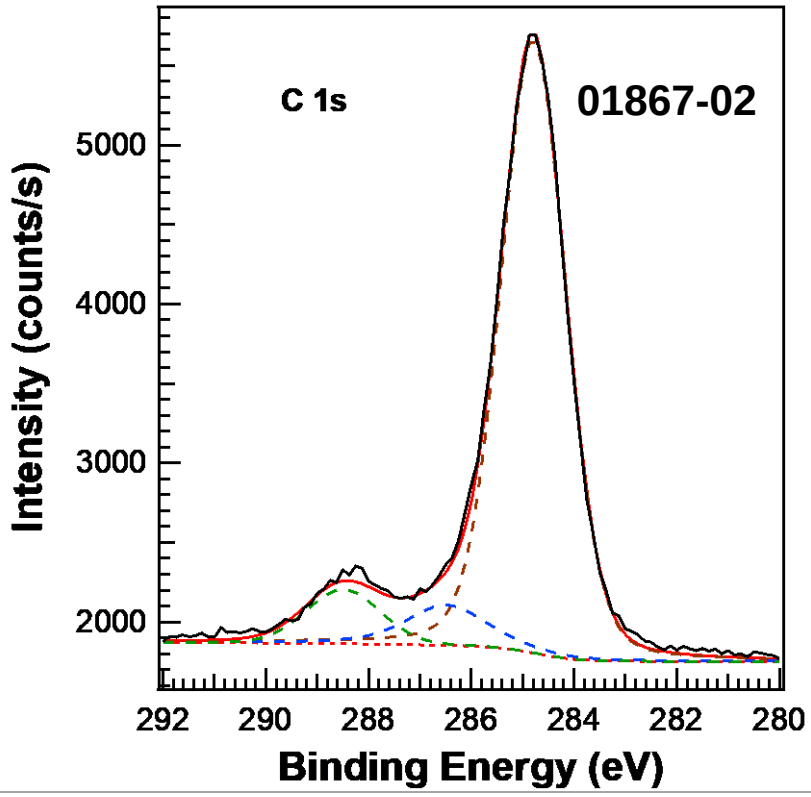

Publish in *SSS*: Yes X No ☐

- **Accession #:** 01867-02
- **Host Material:** Fe_2O_3-gCN(CM)
- **Technique:** XPS
- **Spectral Region:** C 1s

Instrument: PHI 5000 Versaprobe
Excitation Source: Al Ka monochromatic
Source Energy: 1486.6 eV
Source Strength: 100 W
Source Size: 0.2 mm x 0.2 mm
Analyzer Type: spherical sector
Incident Angle: 0˚
Emission Angle: 45˚
Analyzer Pass Energy 58.7 eV
Analyzer Resolution: 0.6 eV
Total Signal Accumulation Time: 740.0 s
Total Elapsed Time: 814.0 s

Number of Scans: 80

Effective Detector Width: 0.6 eV

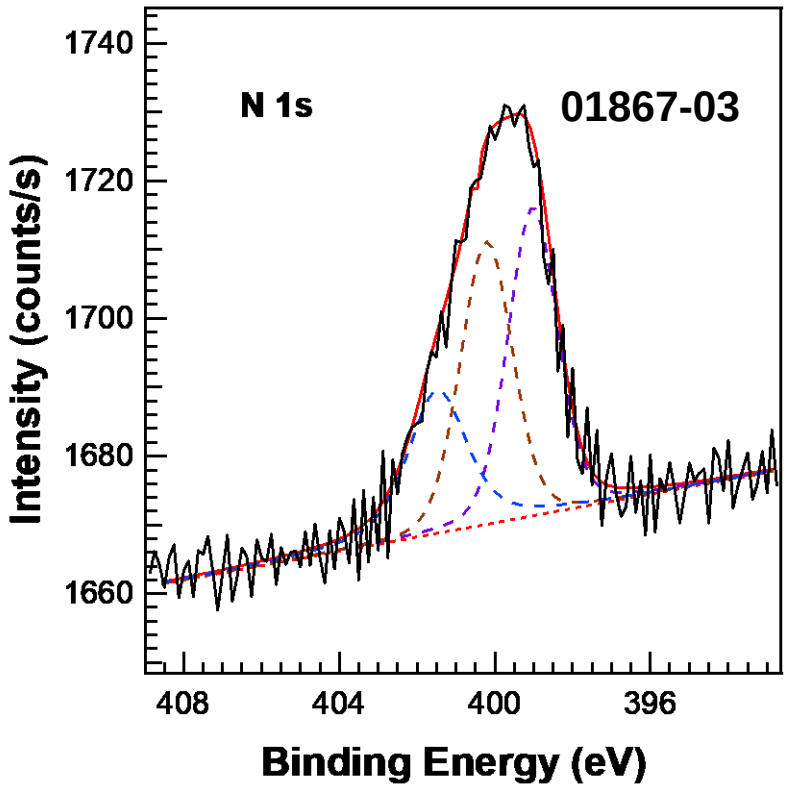

Publish in *SSS*: Yes X No ☐

- **Accession #:** 01867-03
- **Host Material:** Fe_2O_3-gCN(CM)
- **Technique:** XPS
- **Spectral Region:** N 1s

Instrument: PHI 5000 Versaprobe
Excitation Source: Al Ka monochromatic
Source Energy: 1486.6 eV
Source Strength: 100 W
Source Size: 0.2 mm x 0.2 mm
Analyzer Type: spherical sector
Incident Angle: 0˚
Emission Angle: 45˚
Analyzer Pass Energy 58.7 eV
Analyzer Resolution: 0.6 eV
Total Signal Accumulation Time: 2080.0 s
Total Elapsed Time: 2288.8 s

Number of Scans: 320

Effective Detector Width: 0.6 eV

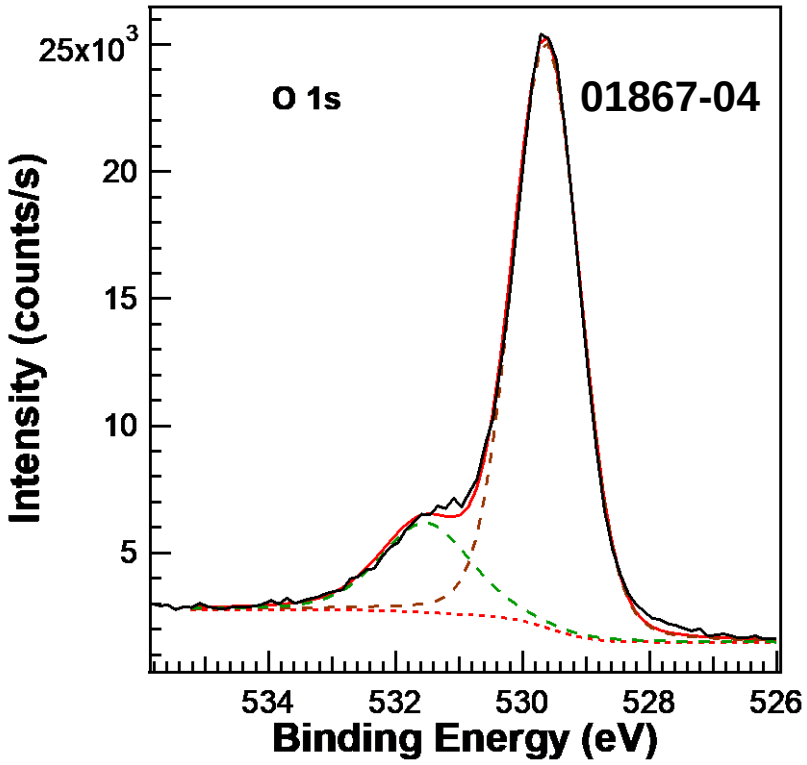

Publish in *SSS*: Yes X No ☐

- **Accession #:** 01867-04
- **Host Material:** Fe_2O_3-gCN(CM)
- **Technique:** XPS
- **Spectral Region:** O 1s

Instrument: PHI 5000 Versaprobe
Excitation Source: Al Ka monochromatic
Source Energy: 1486.6 eV
Source Strength: 100 W
Source Size: 0.2 mm x 0.2 mm
Analyzer Type: spherical sector
Incident Angle: 0˚
Emission Angle: 45˚
Analyzer Pass Energy 58.7 eV
Analyzer Resolution: 0.6 eV
Total Signal Accumulation Time: 70.8 s
Total Elapsed Time: 77.9 s

Number of Scans: 8

Effective Detector Width: 0.6 eV

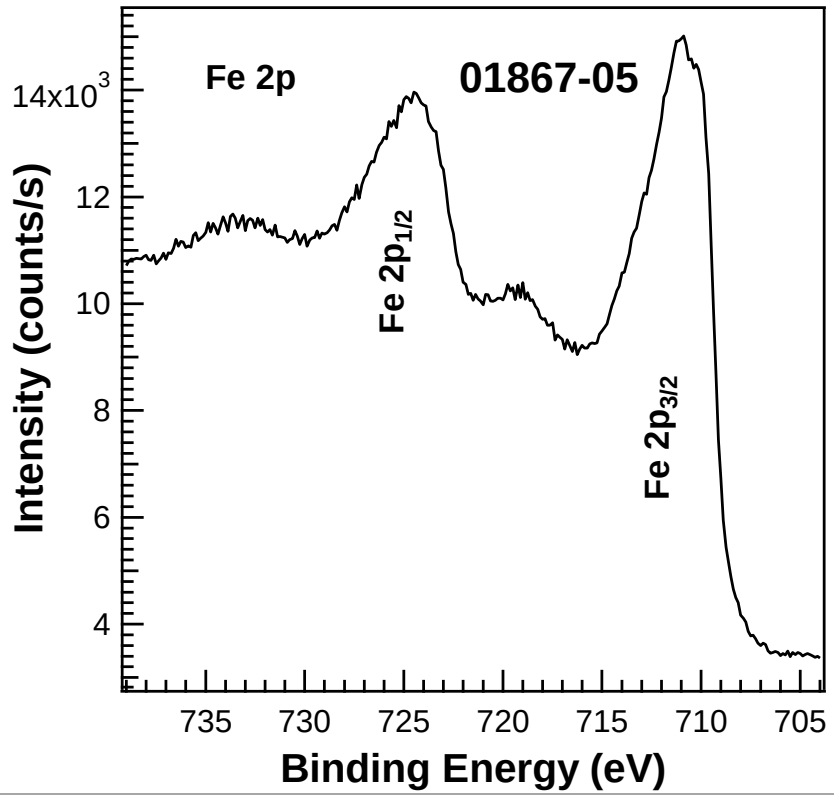

Publish in *SSS*: Yes X No ☐

- **Accession #:** 01867-05
- **Host Material:** Fe_2O_3-gCN(CM)
- **Technique:** XPS
- **Spectral Region:** Fe 2p

Instrument: PHI 5000 Versaprobe
Excitation Source: Al Ka monochromatic
Source Energy: 1486.6 eV
Source Strength: 100 W
Source Size: 0.2 mm x 0.2 mm
Analyzer Type: spherical sector
Incident Angle: 0˚
Emission Angle: 45˚
Analyzer Pass Energy 58.7 eV
Analyzer Resolution: 0.6 eV
Total Signal Accumulation Time: 513.6 s
Total Elapsed Time: 565.0 s

Number of Scans: 32

Effective Detector Width: 0.6 eV